

Highlights from STAR

Xin Dong (for the STAR Collaboration)¹

*Lawrence Berkeley National Laboratory
MS70R0319, 1 Cyclotron Road, Berkeley, CA 94720, USA*

Abstract

In these proceedings, I highlight some selected results from the STAR experiment that were presented in the Quark Matter 2012 conference.

1. Introduction

The physics program of the STAR experiment covers various aspects of QCD frontiers. Diverse heavy ion collisions provided by the RHIC machine allow us to systematically study the properties of the strongly-coupled Quark Gluon Plasma (sQGP) at the top RHIC energy, as well as to map out the phase structure of QCD matter by scanning the phase diagram with variable collision energies. The $p(d)$ -A collisions provide opportunities to control the cold nuclear effects and to study the QCD in the low- x regime.

The STAR detector at RHIC is well suited to carry out these physics programs [1]. A side view of the STAR detector and its main subsystems are shown in the left plot of Fig. 1. The STAR detector has a large and uniform acceptance with excellent particle identification at mid-rapidity ($|\eta| < \sim 1$) across all collider energies. The calorimeter subsystems extend to forward

¹A list of members of the STAR Collaboration and acknowledgements can be found at the end of this issue.

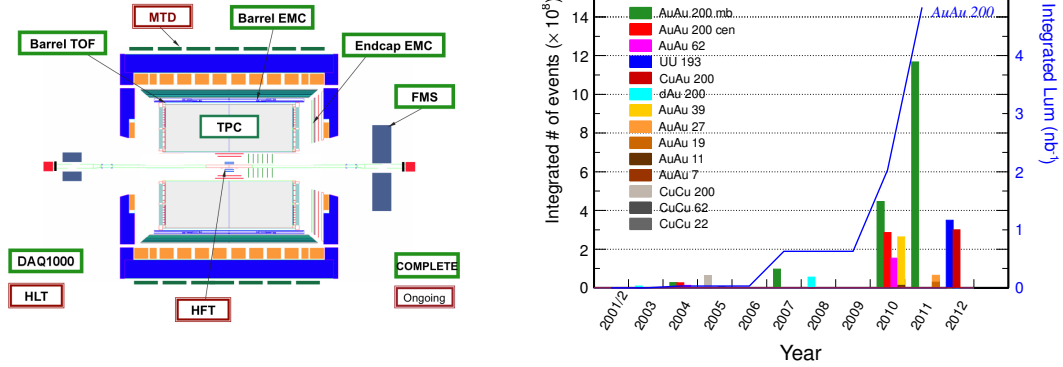


Figure 1: (Left): A side view of the STAR detector and its main subsystems. (Right): Heavy-ion minimum bias/central data sets (histograms) and integrated luminosity (line) recorded by the STAR detector.

rapidity (up to $\eta \sim 4$) enabling to probe extreme kinematic regions. Figure 1 right panel shows the recorded heavy ion data samples from all RHIC runs by the STAR detector. Significant amounts of data have been accumulated since 2010 when the fast data acquisition and the TOF subsystem upgrades were completed. STAR has entered the era of precision measurements to study the QCD in hot and cold nuclear matter.

In these proceedings, I will highlight some selected STAR results that were presented in the Quark Matter 2012 conference. Please refer to the STAR contributed articles in these proceedings for more details.

2. Forward dihadron correlations to search for the Color Glass Condensate (CGC)

The gluon density within a hadron increases drastically with decreasing x , but will saturate when gluon recombination balances gluon splitting and the collinear factorization fails. This idea has been casted in a precise theoretical

28 frame known as Color Glass Condensate (CGC) effective theory model [2].
 29 The saturation scale (Q_s^2) at a given x increases as $A^{1/3}$, thus it becomes more
 30 effective to search for this phenomena using collisions with nuclei. At the
 31 leading order $2 \rightarrow 2$ process, triggering the produced particle in the forward
 32 region and varying the associated particle η regions offers an opportunity
 33 to study the x dependence of particle production enabling to probe regimes
 34 from dilute parton gas to possible CGC. Previously, STAR has reported the
 35 measurement of forward π^0 - π^0 correlations in the rapidity region $2.5 < \eta < 4$
 36 with the FMS detector. The back-to-back correlation in $d + \text{Au}$ collisions
 37 is significantly suppressed or broadened compared to that in $p + p$ collisions,
 38 consistent with the CGC expectation [3]. The measurement of forward ($2.5 <$
 39 $\eta < 4$) and mid rapidity ($-1 < \eta < 1$) π^0 correlations show no significant
 40 difference in the correlation widths between $p + p$ and $d + \text{Au}$ collisions [3].

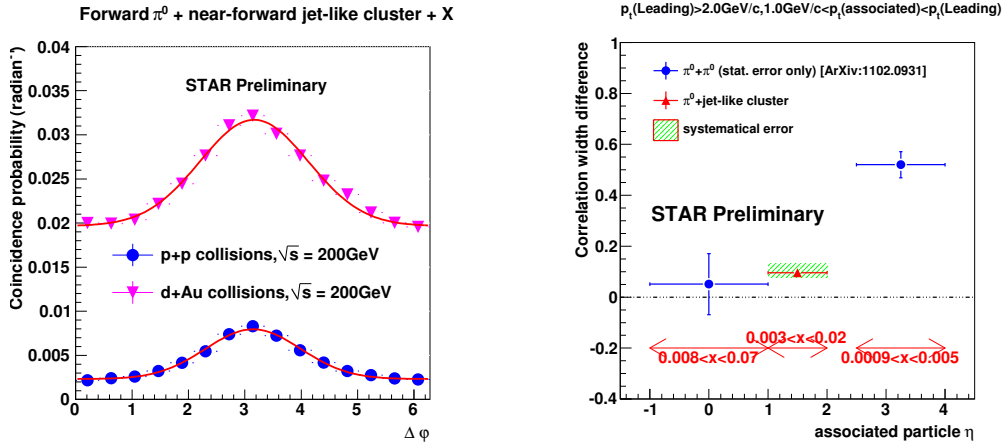


Figure 2: (Left): Dihadron azimuthal angle difference $\Delta\phi$ distributions between forward π^0 triggered by FMS ($2.5 < \eta < 4$ and near-forward jet-like cluster from EEMC ($1 < \eta < 2$) in $p + p$ and $d + \text{Au}$ collisions at $\sqrt{s_{NN}} = 200$ GeV. (Right): Correlation width difference between $p + p$ and $d + \text{Au}$ triggered by the FMS π^0 vs. the associated particle η .

41 In this conference, we report the dihadron correlation measurement with
 42 forward π^0 from FMS and near-forward ($1 < \eta < 2$) jet-like cluster from
 43 EEMC [4]. It is sensitive to the intermediate x region to study the transi-
 44 tion between previous forward-forward and forward-midrapidity correlations.
 45 The correlation distributions in $p + p$ and $d + \text{Au}$ collisions at $\sqrt{s_{NN}} = 200$
 46 GeV are shown in the left plot of Fig. 2. Red lines depict gaussian fits to two
 47 distributions to extract the widths. The width difference between $d + \text{Au}$
 48 and $p + p$ from forward triggered correlations with associated particles com-
 49 ing from different η regions is summarized in the right plot of Fig. 2. Also
 50 shown in the plot are the corresponding gluon x regions in the Au nuclei
 51 for correlations with different associate particle η . The plot shows that with
 52 increasing associate particle η - and thus smaller gluon x - the correlation
 53 width difference increases. The x dependence feature in forward dihardon
 54 correlations is consistent with a smooth transition from the dilute parton gas
 55 to the CGC regime.

56 **3. Towards precision understanding of the sQGP properties**

57 The strong elliptic flow (v_2) and the number of constituent quark (NCQ)
 58 scaling found for multi-strange hadrons at RHIC top energy are clear evidence
 59 of partonic collectivity, a critical feature of the sQGP [5]. With the unprece-
 60 dented statistics collected in the past years, STAR is able to make systematic
 61 measurements to study the partonic collectivity and to investigate the sQGP
 62 properties [6]. Figure 3 shows the recent v_2 measurements of identified parti-
 63 cles ($\pi^\pm, K^\pm, K_S^0, p, \bar{p}, \phi, \Lambda, \bar{\Lambda}, \Xi^-, \bar{\Xi}^+, \Omega^-, \bar{\Omega}^+$) as a function of transverse kinetic
 64 energy $m_T - m_0$ from Au + Au 200 GeV minimum bias (left), 0-30% (middle)

65 and 30-80% (right) centrality collisions, respectively. In minimum bias and
 66 0-30% centrality, the measurements show a clear baryon/meson grouping and
 67 the NCQ scaling holds within 10% for all particles at $(m_T - m_0)/n_q > 0.6$
 68 GeV/c^2 , suggesting that partonic collectivity dominates the final observed v_2 .
 69 While in 30-80% centrality, one can see the baryon/meson grouping starts
 70 to collapse, and the v_2/n_q of multi-strange hadrons (ϕ, Ξ) deviates from that
 71 of K_S^0 beyond 10-15%, suggesting smaller contributions from the partonic
 72 phase to the final collectivity. We also report systematic measurements of
 73 all hadronic flows for charged hadrons up to $n = 5$ [7]. All these systematic
 74 measurements provide significant inputs to constrain the sQGP properties
 75 when comparing to hydrodynamic model calculations.

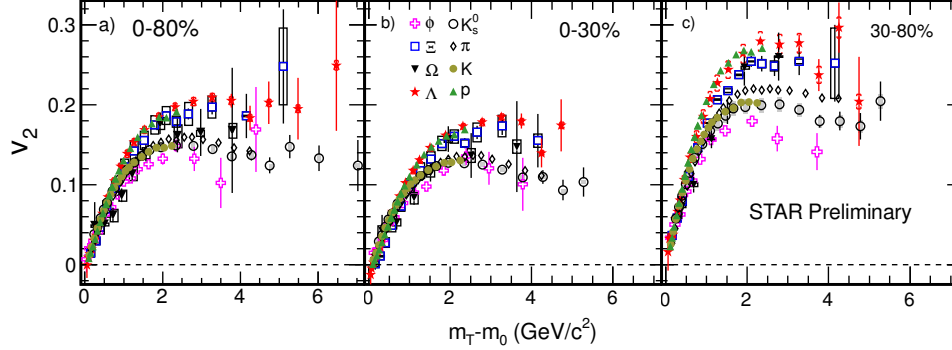


Figure 3: Identified particle v_2 vs. transverse kinetic energy $(m_T - m_0)$ in Au + Au 200 GeV for 0-80% minimum bias (a), 0-30% (b) and 30-80% (c) centrality bins. Error bars on the data points are statistical, and caps, open or shaded boxes are systematic uncertainties on different particles for better illustration.

76 In 2012, RHIC for the first time collided two uranium beams. The ura-
 77 nium nucleus has a much larger mass and is largely deformed. It is very

78 interesting to study the sQGP properties at higher particle density as well
 79 as with different collision orientations. Figure 4 left plot shows the inte-
 80 grated charged hadron v_2 using the η -sub event plane method vs. uncorrected
 81 charged particle density $dN_{ch}/d\eta$ in the region of $0.15 < p_T < 2$ GeV/ c and
 82 $|\eta| < 1$ from 200 GeV Au + Au and 193 GeV U + U collisions [8]. One
 83 can see in the central and mid-central collisions, the v_2 in U + U collisions
 84 is always higher than that in Au + Au collisions at the same uncorrected
 85 $dN_{ch}/d\eta$.

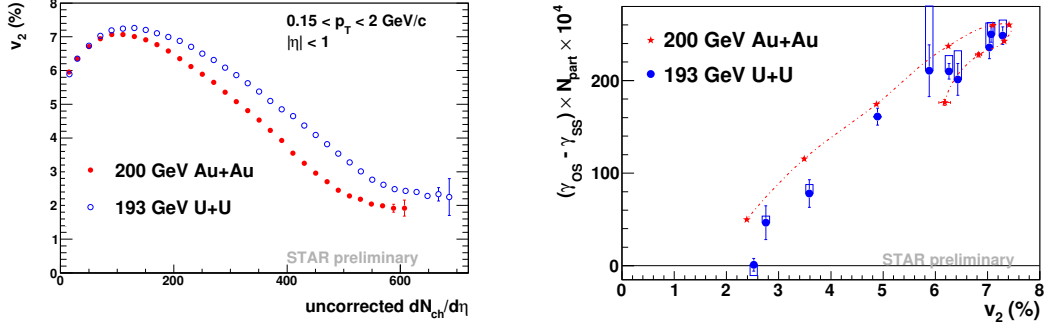


Figure 4: (Left) Charged hadron v_2 vs. uncorrected $dN_{ch}/d\eta$ for Au + Au 200 GeV and U + U 193 GeV collisions. (Right) Charge separation signal w.r.t. the event plane $(\gamma_{OS} - \gamma_{SS})$ from Au + Au (red) and U + U collisions (blue). The most left blue data point was obtained from the 0-1% central triggered U + U collisions. Boxes depict the systematic uncertainties due to the possible pileup background source.

86 STAR previously reported the measurement of the charge separation with
 87 respect to the event plane, which was motivated by the search for the par-
 88 ity violation in strong interactions and the chiral magnetic effect (CME) in
 89 heavy ion collisions [9]. There was some discussion on the physics back-
 90 ground caused by the local energy/momentum conservation convoluted with
 91 the event-by-event elliptic flow [10]. U + U collisions provide an opportunity

92 to test the validation of the CME signal with tuning the magnitudes in v_2
 93 and the magnetic field by different collision orientations [11]. Figure 4 right
 94 plot shows the charge separation signal w.r.t. the event plane (difference
 95 between $\gamma \equiv \langle \cos(\phi_a + \phi_b - 2\Psi_{\text{RP}}) \rangle$ for opposite sign and same sign pairs)
 96 vs. the measured v_2 in Au + Au and U + U collisions. One particular note
 97 is that the most left data point in U + U collisions was obtained from the
 98 0-1% central triggered data sample where the magnetic field is expected to be
 99 significantly suppressed. The result is consistent with zero while there is still
 100 a sizable v_2 ($\sim 2.5\%$) in 0-1% central collisions. The observation is consistent
 101 with no signal when the magnetic field is turned off, which is expected from
 102 the CME [8].

103 Heavy flavors are ideal probes to study the sQGP properties because of
 104 higher sensitivity due to their large masses. STAR previously reported open
 105 charm hadron measurements via hadronic decay channels in $p + p$ and Au
 106 + Au collisions at 200 GeV [12]. With significantly improved statistics from
 107 year 2011 Au + Au collisions, we are able to carry out more systematic
 108 measurements on the charm total cross section as well as the $D^0 R_{AA}$ [13].
 109 Figure 5 left plot shows the charm production cross section per nucleon-
 110 nucleon collision from $p + p$ to central Au + Au collisions. The data points
 111 from Au + Au collisions were extracted from the measurement of D^0 mesons
 112 assuming the same fragmentation ratio ($c \rightarrow D^0$) as in $p + p$. The results,
 113 with significantly improved precision, still show the charm total cross section
 114 follows the binary scaling from $p + p$ to central Au + Au collisions.

115 Figure 5 right plot shows the R_{AA} of D^0 mesons in central and minimum
 116 bias Au + Au collisions covering $0 < p_T < \sim 6$ GeV/ c . Two important

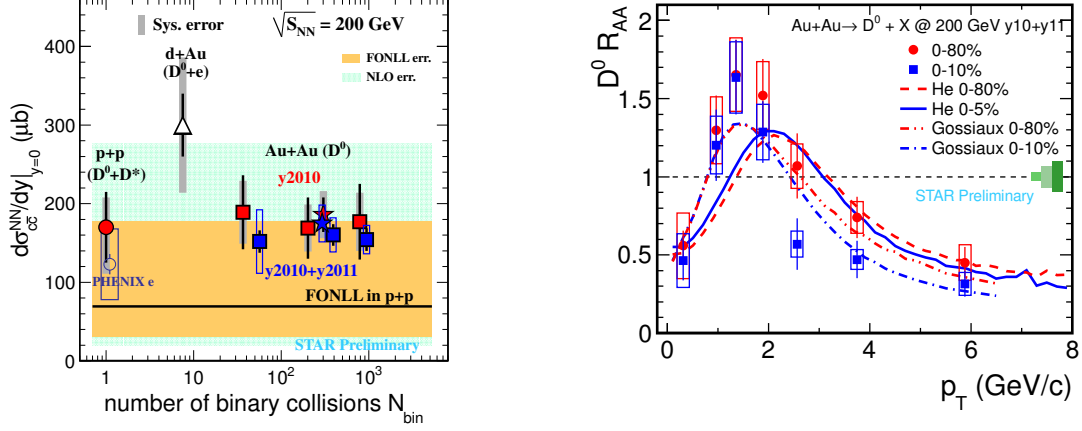


Figure 5: (Left): Charm production cross section per nucleon-nucleon collision from $p + p$ to central Au + Au collisions at 200 GeV; (Right): The D^0 meson R_{AA} vs. p_T for 0-10% and 0-80% centralities in Au + Au collisions at $\sqrt{s_{NN}} = 200$ GeV compared to two transport model calculations. Error bars on the data points are statistical while boxes are systematic uncertainties.

117 features: the data points show a modified hump structure at about 1 – 3
 118 GeV/ c , which may indicate strong interactions between charm quarks with
 119 the medium; at $p_T > 3$ GeV/ c , there is a strong suppression in the observed
 120 $D^0 R_{AA}$, and the suppression is larger in central collisions, indicating large
 121 energy loss for the energetic charm quarks traversing through the medium.
 122 Also shown on the plot are two transport model calculations which reasonably
 123 describe the measured data points [14].

124 Dilepton pairs produced from the fireball carry clean information and of-
 125 fer insights into medium properties at different stages [15]. STAR presented
 126 the dielectron production in 200 GeV Au + Au collisions at QM11, and re-
 127 ported a sizable enhancement compared to the hadronic cocktail in the mass
 128 region of 0.3-0.7 GeV/ c^2 [16]. The excess can be described by a broadened ρ

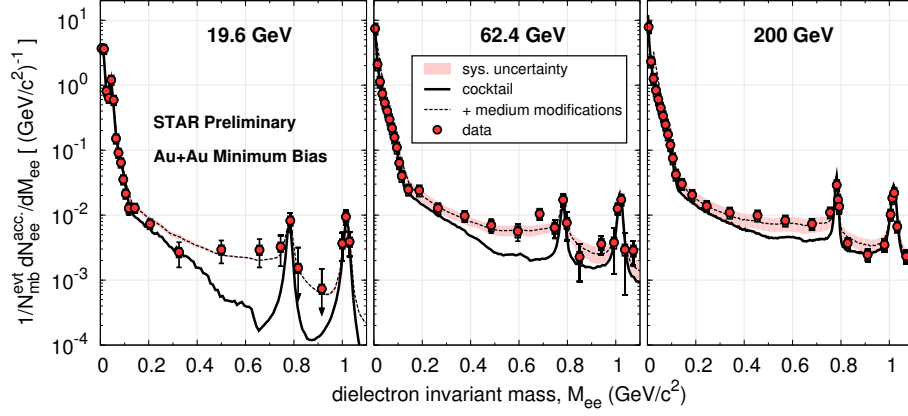


Figure 6: Dielectron mass spectra from Au + Au collisions at $\sqrt{s_{NN}} = 19.6, 62.4$ and 200 GeV compared to the hadronic cocktail plus the medium vector meson and QGP contributions from model calculations. Uncertainties on the data points include statistical (bars) and systematical (boxes) and the red bands depict the uncertainties of cocktails.

129 in the hadronic medium [15, 17]. We have continued with more differential
 130 measurements and have studied the p_T and centrality dependence as well as
 131 elliptic flow at 200 GeV [18]. We also carried out a systematic measurement
 132 of the dielectron yield at various beam energies (19.6, 39, 62.4 GeV). Fig-
 133 ure 6 shows the dielectron mass spectrum within the STAR acceptance in
 134 Au + Au collisions at $\sqrt{s_{NN}} = 19.6, 62.4$ and 200 GeV. The data show that
 135 the enhancement in the low mass region compared to the hadronic cocktail
 136 persists in all energies. Also included in the plot are calculated contributions
 137 of in-medium ρ together with the QGP radiation from [15]. The low mass
 138 excess can be consistently accounted for by the broadened ρ production in
 139 the hadronic medium from 19.6 to 200 GeV.

140 4. Results from Beam Energy Scan (BES) program

141 To study the QCD phase structure and locate the first-order phase tran-
 142 sition as well as a possible critical point [19], RHIC has started the Beam
 143 Energy Scan (BES) program and the phase-I data have been taken in 2010
 144 and 2011 with Au + Au collisions at energies of 39, 27, 19.6, 11.5, and 7.7
 145 GeV.

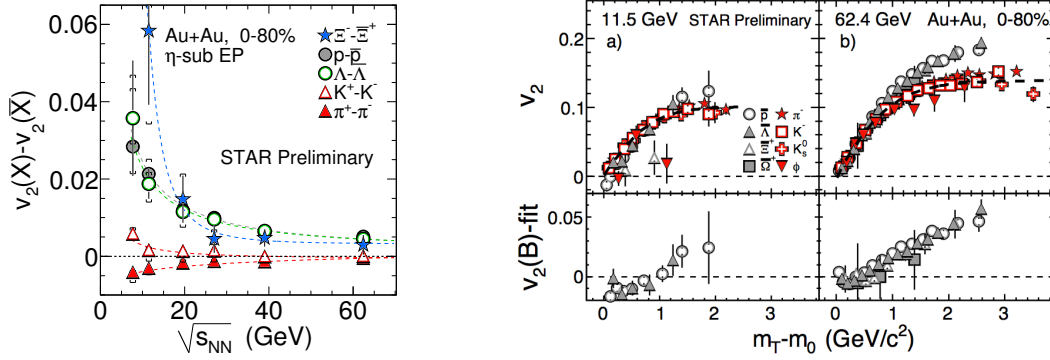


Figure 7: (Left): Particle and anti-particle v_2 difference vs. collision energy. Uncertainties on data points are statistical (bars) and systematical (brackets). (Right): Identified particle v_2 vs. $m_T - m_0$ for anti-particles in Au + Au collisions at 11.5 GeV and 62.4 GeV. Error bars are statistical only.

146 One of the first questions when we lower the collision energies is whether
 147 these key sQGP signatures observed at the top RHIC energy turn off. Ellip-
 148 tic flow of identified particles and the NCQ scaling test have been proposed
 149 to address this question. We have made systematic measurements for iden-
 150 tified particle v_2 in all beam energies [20]. Strikingly, we observed that the
 151 difference in v_2 between particles and anti-particles, which is negligible at top
 152 RHIC energy, starts to increase with decreasing collision energy, shown in the

153 left plot of Fig. 7. The difference for baryons is larger than mesons. This sug-
 154 gests the breakdown of the NCQ scaling between particles and anti-particles
 155 at lower energies. In addition, we also observe that for anti-particles, the
 156 baryon/meson grouping at intermediate p_T starts to collapse at 11.5 GeV,
 157 shown on the right plot of Fig. 7. These observations indicate that hadronic
 158 interactions become more dominant at lower beam energies. We also observed
 159 changes of other key sQGP features at lower energies, e.g., the disappearance
 160 of high p_T suppression [21, 22] and the charge separation signal [8].

161 Directed flow (v_1) of protons has been proposed as a sensitive probe to
 162 the softening of the equation of state and/or the first order phase transition.
 163 STAR made systematic measurements of v_1 of identified particles [7]. The
 164 rapidity dependence of v_1 , often quantified as the slope parameter dv_1/dy'
 165 ($y' \equiv y/y_{\text{beam}}$) vs. collision energy in Au + Au collisions from 10-40% cen-
 166 trality are plotted in Fig. 8. We observe that the proton v_1 slope changes
 167 sign from positive to negative when the collision energy increases from 7.7
 168 GeV to 11.5 GeV, and it rises with increasing energy, but stays negative
 169 and approaches zero at 200 GeV. The v_1 slopes of other particles (\bar{p} , π^\pm ,
 170 K^\pm) are all negative in our measured energy region. In the bottom panel of
 171 Fig. 8, we take the difference in the slope parameters between protons and
 172 anti-protons weighted by their relative production yields, *i.e.* “net-proton” v_1
 173 slope. A striking observation is that the net-proton v_1 changes sign twice in
 174 the measured energy region, and shows a minimum between 11.5-19.6 GeV.
 175 Also shown on the figure are transport model calculations. However, neither
 176 of these calculations can reproduce the observed net-proton v_1 slope. Other
 177 physics sources are under investigation.

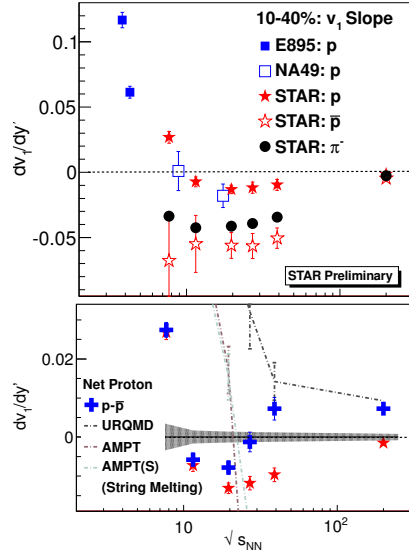


Figure 8: (Upper) Directed flow v_1 slope parameter of p , \bar{p} and π^- vs. energy. (Lower) net-proton v_1 slope parameter vs. energy and compared to transport model calculations. Error bars are statistical only.

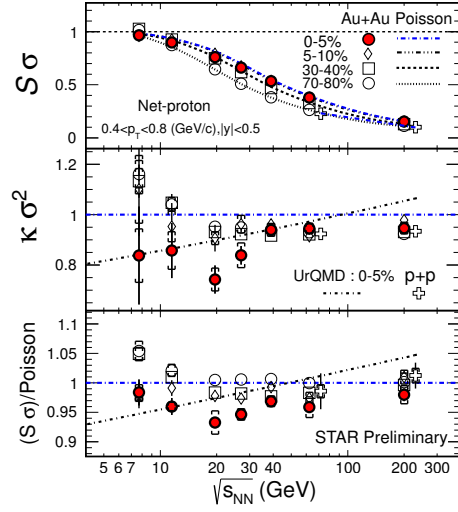


Figure 9: Moment products $S\sigma$, $\kappa\sigma^2$ of net-proton multiplicity in various collision centralities in Au + Au collisions from $\sqrt{s_{NN}} = 7.7$ - 200 GeV. The data points are compared to the Poisson expectation values and the bottom panel shows the ratio of $S\sigma$ over the Poisson expectation. Uncertainties included are statistical (bars) and systematical (brackets).

178 System at the QCD critical point region is expected to show a sharp in-
 179 crease in the correlation length, thus induce large non-statistical fluctuation.
 180 Higher moments of conserved quantities (e.g. net-baryon number) are pro-
 181 posed to be an ideal probe as they are more sensitive to the critical point
 182 induced fluctuations [23]. A non-monotonic behavior of high moment distri-
 183 butions vs. collision energy is expected to be a signature of the QCD critical
 184 point. In Fig. 9, we present the STAR measurements of moment products
 185 $S\sigma$ and $\kappa\sigma^2$ of net-proton multiplicity distributions in various collision cen-
 186 tralities in Au + Au collisions from 7.7 to 200 GeV [24]. Also plotted in the
 187 figure are the Poisson expectations in the first two panels and the ratio of $S\sigma$
 188 over the Poisson expectation is shown in the bottom panel. We observe that
 189 in 0-5% central collisions, moment products deviate from Poisson expecta-
 190 tion at $\sqrt{s_{NN}} > 7.7$ GeV, while in peripheral collisions, the data points are
 191 above the Poisson expectation below 19.6 GeV. The UrQMD transport model
 192 calculations show a monotonic behavior with collision energy. Data points
 193 below 19.6 GeV have large uncertainties which prevents us from drawing a
 194 conclusion on the energy dependence behavior. Details of other fluctuation
 195 measurements can be found in [25].

196 STAR has completed the BES phase-I. We have observed many signifi-
 197 cantly different features compared to top RHIC energy. To locate the QCD
 198 phase boundary and the critical point, we need more precise measurements
 199 focusing at the energy region $\sqrt{s_{NN}} < \sim 20$ GeV.

200 5. Outlook

201 STAR has just entered the era of precision QCD measurements. In the
202 next decade, we have outlined a set of fruitful and compelling science pro-
203 grams with upgrades on both the detector subsystems and the RHIC ma-
204 chine [26]. In the near term, STAR has two major subsystem upgrades
205 - the Heavy Flavor Tracker and the Muon Telescope Detector - targeting
206 for precision measurements on heavy flavors and dileptons to measure the
207 sQGP properties. The current exciting but inconclusive BES results call for
208 the BES phase-II program of precision measurements to map out the QCD
209 phase structure. In the long term, STAR is exploring the upgrades at for-
210 ward/backward regions to expand our physics program in $p(e)$ -A collisions
211 to precisely study QCD in the cold nuclear matter.

212 References

213 References

- 214 [1] K.H. Ackermann *et al.*, Nucl. Instrum. Meth. A 499 (2003) 624.
- 215 [2] F. Gelis, E. Lancu, J. Jalilian-Marian and R. Venugopalan, Ann. Rev.
216 Nucl. Part. Sci. 60 (2010) 463.
- 217 [3] E. Braidot (for the STAR Collaboration), Nucl. Phys. A. 854 (2011)
218 168.
- 219 [4] X. Li (for the STAR Collaboration), these proceedings.
- 220 [5] B.I. Abelev *et al.*, Phys. Rev. Lett. 99 (2007) 112301.

- 221 [6] M. Nasim (for the STAR Collaboration), these proceedings.
- 222 [7] Y. Pandit (for the STAR Collaboration), these proceedings.
- 223 [8] G. Wang (for the STAR Collaboration), these proceedings.
- 224 [9] B.I. Abelev *et al.*, Phys. Rev. Lett. 103 (2009) 251601; B.I. Abelev *et*
225 *al.*, Phys. Rev. C 81 (2010) 054908.
- 226 [10] S. Pratt, arXiv: 1002.1758.
- 227 [11] S.A. Voloshin, Phys. Rev. Lett. 105 (2010) 172301.
- 228 [12] Y. Zhang (for the STAR Collaboration), J. Phys. G 38 (2011) 124142.
- 229 [13] D. Tlusty (for the STAR Collaboration), these proceedings.
- 230 [14] M. He, R.J. Fries, R. Rapp, arXiv: 1204.4442; P.B. Gossiaux *et al.*,
231 arXiv: 1207.5445.
- 232 [15] R. Rapp, Adv. Nucl. Phys. 25 (2000) 1; arXiv: nucl-th/0204003; private
233 communications.
- 234 [16] J. Zhao (for the STAR Collaboration), J. Phys. G 38 (2011) 124134.
- 235 [17] O. Linnyk *et al.*, Phys. Rev. C 85 (2012) 024910; H. Xu *et al.*, Phys.
236 Rev. C 85 (2012) 024906.
- 237 [18] B. Huang (for the STAR Collaboration), these proceedings.
- 238 [19] M.M. Aggarwal *et al.*, arXiv: 1007.2613.
- 239 [20] S. Shi (for the STAR Collaboration), these proceedings.

- 240 [21] E. Sangaline (for the STAR Collaboration), these proceedings.
- 241 [22] X. Zhang(for the STAR Collaboration), these proceedings.
- 242 [23] M.A. Stephanov, Phys. Rev. Lett. 107 (2011) 052301.
- 243 [24] X. Luo (for the STAR Collaboration), these proceedings.
- 244 [25] L. Chen (for the STAR Collaboration), these proceedings; D. McDonald
245 (for the STAR Collaboration), these proceedings; P. Tribedy (for the
246 STAR Collaboration), these proceedings.
- 247 [26] H. Huang (for the STAR Collaboration), these proceedings.